CrossMark

JM PAPERS

Upscale transfer of waves in one-dimensional rotating shallow water

Jim Thomas[1,2,†] and Lingyun Ding[3]

[1]International Centre for Theoretical Sciences, Tata Institute of Fundamental Research, Bangalore 560089, India

[2]Centre for Applicable Mathematics, Tata Institute of Fundamental Research, Bangalore 560065, India

[3]Department of Mathematics, University of California, Los Angeles, CA 90095, USA

We study the inverse flux of waves in one of the simplest geophysical fluid dynamics models: one-dimensional rotating shallow water equations. Based on direct numerical integration of the governing equations, we find that waves injected at small scales get transferred upscale predominantly via resonant quartic interactions between wave modes. The waves' upscale transfer is non-local and involves turbulent transfer between disparate scales of the flow. Our analysis reveals that the upscale transfer of waves is extremely intermittent and is a result of localized-in-time bursts in wave action flux. These intermittent events of flux bursts lead to shallower waves' spectrum and relatively higher amplitude wave fields in physical space. On examining statistics of the flow fields, we find that low-energy high wavenumbers more or less comply with the assumptions used in wave turbulence theory, such as uniformly distributed wave phases and the Gaussian distribution of fields, while non-uniform distribution of wave phases and non-Gaussian statistics dominate at large scales or low wavenumbers that contain a major share of the flow energy. Our findings point out that the one-dimensional rotating shallow water equations, despite being a simple geophysical fluid dynamic model, harbour complex and intricate features associated with the upscale transfer of waves that have not been recognized in the past.

Key words: waves in rotating fluids, shallow water flows, rotating turbulence

1. Introduction

Dispersive waves are ubiquitous in geophysical flows, such as flows in the atmosphere and world's oceans. These waves can spontaneously generate slowly evolving mean flows, enhance turbulent diffusivity of flows and are hypothesized to form an energy sink for balanced vortical flows (Bretherton 1969; Francois *et al.* 2014; Suanda *et al.* 2018; Xia *et al.* 2019; Thomas & Daniel 2020, 2021; Thomas & Gupta 2022). The balanced

† Email address for correspondence: jimthomas.edu@gmail.com

vortical mode in geophysical flows contain a major fraction of the total flow energy and mechanisms by which such mean flows can dissipate their energy is an unresolved question. Additionally, the irreversible modification of vortical flows by the presence of energetic dispersive waves is thought of as a means by which the lateral diffusivity of oceanic flows can be increased (Shcherbina *et al.* 2015). Turbulent exchanges between fast dispersive waves and slow vortical mean flows is therefore an active research area in geophysical fluid dynamics, with investigations focusing on potential mechanisms by which dispersive waves can form an energy sink for slow mean vortical flows and enhance local turbulent flow diffusivity.

Further to energy exchanges with slow mean flows and enhancing flow diffusivity, the turbulent dynamics of dispersive waves in geophysical flows are investigated to understand detailed mechanisms by which wave energy is transferred from large inviscid to small dissipative scales (Muller *et al.* 2015; Dong, Bühler & Smith 2020; Pollmann 2020). While vortical flows generically transfer energy upscale via an inverse energy flux, waves transfer energy downscale via a forward energy flux. This wave energy transfer from large to small scales is the predominant mechanism by which small scale mixing takes place in geophysical flows, especially in the world's oceans. Consequently, resolving mechanisms that trigger the forward flux of waves and identifying localized regions where waves dissipate are imperative for developing better parametrizations for large-scale atmosphere–ocean–climate models that are far from resolving the dynamics of a broad spectrum of fast dispersive waves (Garrett & Kunze 2007; Alford *et al.* 2016; Moum 2021).

When compared with the above-mentioned interests and investigations into the energy exchanges of waves with vortical flows, wave-induced modification of flow diffusivity and the forward flux of waves, the least studied aspect of dispersive waves in geophysical flows is the upscale or inverse flux of waves. The inverse flux of waves is a non-trivial and counterintuitive feature that is specific to waves whose dispersion relationship does not allow resonant triads. Such wave systems, with deep water surface gravity waves and inertia-gravity waves in a shallow rotating fluid being popular examples, conserve wave action in addition to wave energy (Nazarenko 2011). The conservation of wave action and wave energy results in two kinds of turbulent transfers: a forward flux of wave energy and an inverse flux of wave action. The phenomenology is qualitatively analogous to that in two-dimensional hydrodynamic turbulence and quasi-geostrophic turbulence characterized by an upscale energy transfer and a downscale enstrophy transfer (Salmon 1978; Vallis 2006).

Theoretical calculations based on the weakly nonlinear wave turbulence formalism predicts the inverse flux of surface gravity waves (Zakharov, L'vov & Falkovich 1992), and in recent times a broad set of studies have examined this upscale wave transfer using direct numerical integration of the governing equations and laboratory experiments (Annenkov & Shrira 2006; Korotkevitch 2008; Deike, Laroche & Falcon 2011; Falcon *et al.* 2020). A key outcome of these and related studies is the appreciation that weakly nonlinear turbulent wave fields can exhibit significant departures from the idealized states assumed in wave turbulence formalism. Notably, non-Gaussian effects and intermittency in turbulent transfers are features that are generically seen in surface wave turbulence studies (Yokoyama 2004; Falcon, Fauve & Laroche 2007*a*; Falcon, Laroche & Fauve 2007*b*; Falcon *et al.* 2008; Korotkevitch 2008; Falcon, Roux & Laroche 2010). As a result, in addition to confirming some of the predictions of wave turbulence theory, these past studies have shed light on features that are missing in wave turbulence theory; providing theorists new opportunities to further investigate and improve the existing machinery of wave turbulence formalism.

Although the upscale transfer of waves is expected generically for dispersive waves with prohibited triadic interactions, as reflected in the above discussion, most of the upscale wave transfer investigations have focused on surface gravity waves and relatively little is known of inertia-gravity waves in the shallow fluid approximation, as applied to atmospheric and oceanic flows. The rotating shallow water equations (RSWE) capture the dynamics of a thin layer of rotating fluid and are the leading-order approximation for flows in the atmosphere and the ocean (Vallis 2006; Zeitlin 2018). As in the case of surface gravity waves, the inverse flux of inertia-gravity waves in RSWE has been predicted based on theoretical calculations (Falkovich 1992; Falkovich & Medvedev 1992; Glazman 1996). However, the calculations in Falkovich (1992) and Falkovich & Medvedev (1992) use classical wave turbulence theory that overlooks intrinsic features such as intermittency and non-Gaussian statistics, while the calculations in Glazman (1996) includes higher-order wave interaction effects, an adhoc inclusion that does not have a formal asymptotic or a rigorous mathematical justification. Consequently, despite the upscale transfer of inertia-gravity waves being predicted via theoretical calculations three decades back, no confirmation for the phenomenon based on direct numerical integration of the governing equations exist to date.

One-dimensional RSWE is one of the simplest geophysical fluid dynamic models that captures multiple complex features of inertia-gravity waves and has been used consistently in the past to investigate wave-vortex dynamics, forward flux of waves and shock formation, dynamics of geophysical fronts, and the existence and stability of the slow manifold (Kuo & Polvani 1997, 1999; Zeitlin, Medvedev & Polougonven 2003; Bouchut, Le Sommer & Zeitlin 2004). In this paper we investigate the inverse flux of waves and its intricate details in one-dimensional RSWE by direct numerical integration of the governing equations.

We specifically focus on one-dimensional RSWE in this study since the one-dimensional nature of the equations allows us to integrate the model for really long times maintaining high numerical accuracy. As will be seen below, long-time integration of the equations is crucial to the development of statistically steady upscale wave transfers. Additionally, it is noteworthy that significant advances in wave turbulence has been brought out by studying adhoc one-dimensional mathematical models such as the Majda–McLaughlin–Tabak model (Majda, McLaughlin & Tabak 1997) and its generalizations (Cai *et al.* 2001; Zakharov, Dias & Pushkarev 2004). Contrary to such adhoc models, one-dimensional RSWE is a physically relevant model that is often used as a work horse in geophysical fluid dynamic investigations. In this study we aim to explore features associated with the upscale transfer of waves in one-dimensional RSWE.

The plan for the paper is as follows: we present the equations and numerical integration details in § 2, upscale wave transfer results in § 3 and summarize our findings in § 4.

2. Equations, conservation laws, and numerical integration

The RSWE in one dimension are

$$\frac{\partial u}{\partial t} - fv + g\frac{\partial h}{\partial x} + u\frac{\partial u}{\partial x} = 0, \tag{2.1a}$$

$$\frac{\partial v}{\partial t} + fu + u\frac{\partial v}{\partial x} = 0, \tag{2.1b}$$

$$\frac{\partial h}{\partial t} + H\frac{\partial u}{\partial x} + \frac{\partial (hu)}{\partial x} = 0, \tag{2.1c}$$

where (u, v) is the velocity vector, h is the height deviation from the mean height H, f is the rotation rate and g is the acceleration due to gravity. We non-dimensionalize the above equations using

$$x \rightarrow Lx, \quad t \rightarrow \left(\frac{L}{c_0}\right)t, \quad f \rightarrow \left(\frac{c_0}{L}\right)f, \quad (u, v) \rightarrow (\epsilon c_0)(u, v), \quad h \rightarrow (\epsilon H)h.$$
$$(2.2a\text{--}e)$$

In the above non-dimensionalization x coordinate was scaled by a length scale L and L/c_0 was used to scale time, with $c_0 = \sqrt{gH}$ being the non-rotating gravity waves' speed. The velocity was non-dimensionalized by a scale $U = \epsilon c_0$ while the height field fluctuations with respect to the mean were scaled by ϵH. Note that from the velocity scaling we have $\epsilon = U/c_0$. Therefore, ϵ is the Froude number, providing an estimate of how the flow velocity scales with the linear gravity wave speed. Throughout this work we will be based in the weakly nonlinear regime characterized by $\epsilon \ll 1$. Consequently, from the above scaling we have $h \ll H$ (in dimensional form), which means that the fluctuations in the height field are small compared with the mean height. Applying the scaling (2.2a–e) to (2.1) gives us the non-dimensional equations

$$\frac{\partial u}{\partial t} - fv + \frac{\partial h}{\partial x} + \epsilon u \frac{\partial u}{\partial x} = 0, \tag{2.3a}$$

$$\frac{\partial v}{\partial t} + fu + \epsilon u \frac{\partial v}{\partial x} = 0, \tag{2.3b}$$

$$\frac{\partial h}{\partial t} + \frac{\partial u}{\partial x} + \epsilon \frac{\partial (hu)}{\partial x} = 0. \tag{2.3c}$$

In the above equations, f is the non-dimensional rotation rate, based on the scaling described in (2.2a–e).

Inertia-gravity waves and the geostrophically balanced vortical mode form the linear modes of (2.3). In this work we discard the vortical mode and focus on the turbulent dynamics of inertia-gravity waves. The linear waves in (2.3) posses the dispersion relationship

$$\omega_k = \sqrt{f^2 + k^2}. \tag{2.4}$$

Total energy E^ϵ is an integral conserved quantity of (2.3) and is given by the expression

$$E^\epsilon = \int_x \left\{ \tfrac{1}{2}(1 + \epsilon h)\left(u^2 + v^2\right) + \tfrac{1}{2}h^2 \right\} \mathrm{d}x. \tag{2.5}$$

For $\epsilon \ll 1$, the cubic energy expression (2.5) can be approximated by the quadratic energy expression

$$E = \int_x \left\{ \frac{1}{2}\left(u^2 + v^2\right) + \frac{1}{2}h^2 \right\} \mathrm{d}x = \sum_k \left\{ |\hat{u}_k|^2 + |\hat{v}_k|^2 + \left|\hat{h}_k\right|^2 \right\} = \sum_k \hat{E}_k, \tag{2.6}$$

where $(\hat{u}_k, \hat{v}_k, \hat{h}_k)$ is the Fourier transform of (u, v, h). Although the exact energy expression (2.5) is cubic, in the weakly nonlinear regime with $\epsilon \ll 1$, the quadratic and cubic energies are indistinguishable. This was verified in all our numerical integrations and we refer the reader to the Appendix for a detailed confirmation.

The absence of resonant triads is a feature of the inertia-gravity waves' dispersion relationship in (2.4) (see proof of this statement detailed in Babin, Mahalov & Nicolaenko 1997 and Majda 2002). The lack of resonant triads results in the conservation of wave action A given by (Falkovich 1992; Falkovich & Medvedev 1992; Glazman 1996)

$$A = \sum_k \hat{A}_k, \quad \hat{A}_k = \frac{\hat{E}_k}{\omega_k}. \qquad (2.7a,b)$$

It is important to note that the energy $\hat{E}_k$ that appears in (2.7*a,b*) is the quadratic wave energy (2.6), excluding the vortical energy. Since in the present work we exclude the vortical mode, the wave fields are identical to the total fields and wave energy is identical to the total energy. The derivation of the conservation of wave action in (2.7*a,b*) requires writing the solution of the flow variables as the superposition of linear plane waves and then manipulating using the fact that linear waves have no potential vorticity. We omit further details of this derivation that is sketched in Falkovich (1992) and also refer the reader to chapter 8 of Nazarenko (2011) for a more generic derivation applicable to arbitrary systems.

In the absence of the vortical mode, we therefore have conservation of wave energy and wave action. Although the exact energy conserved by RSWE is cubic, as mentioned above, the energy is very well approximated by the quadratic energy in the weakly nonlinear regime. The conservation of wave energy and wave action leads to two kinds of turbulent transfers: a downscale transfer of wave energy and an upscale transfer of wave action. Below we will use numerical integration of the equations to determine features associated with this upscale wave transfer.

2.1. *Numerical integrations*

To examine the upscale transfer of waves, we integrated (2.3) with $\epsilon = 0.1$ using a dealiased pseudospectral scheme in the periodic domain $x \in [0, 2\pi]$. Selected integrations were also performed in a domain twice the size to ensure that domain size did not affect results discussed below. The time integration was performed by using the implicit–explicit third-order Runge–Kutta method detailed in table 6 in Pareschi & Russo (2005). The nonlinear terms were treated explicitly while the dissipative terms described below were treated implicitly. We used the two-thirds dealiasing and denote the maximum wavenumber obtained after dealiasing by k_{max}. Waves were forced in a narrow band centred approximately around $k_{max}/3$. To ensure that the numerical results, especially statistics associated with the waves' transfer in the inertial range, were insensitive to spatio-temporal resolution, we performed a series of numerical integrations with successively increasing resolutions. We first integrated the equations with $k_{max} = 512$. At this spectral resolution the numerical integrations were carried out at successively smaller time steps until the solution was seen to be independent of the time step. Once converged in time, the spectral resolution was doubled and the numerical integrations were carried out again with decreasing time steps. This process was continued until it was confirmed that the resolution $k_{max} = 2048$ generated solutions that were insensitive to further increase in spectral resolution. Specifically, this resolution ensured that details of the turbulent transfer across the inertial range and the associated statistics described in the following section were robust and did not change on further increase in resolution. All the results presented in this paper were therefore generated with the spectral resolution $k_{max} = 2048$.

For the results presented in this paper with the spectral resolution of $k_{max} = 2048$, waves were forced as white noise in a narrow wavenumber band centred at wavenumber 600 as

$597 < k < 603$, with a stochastic forcing scheme, similar to that described in Alvelius (1999). To remove energy accumulating at small grid scales, we added hyperdissipative terms of the form $-\nu\partial^{16}/\partial x^{16}(u, v, h)$ to the right-hand side of (2.3). To ensure that scales to the left of the forcing were free of viscous effects, we set the hyperviscosity ν to 0 for $k \leqslant 640$ and to 10^{-38} for $k > 640$. Linear drag terms of the form $-\gamma(u, v, h)$ were added to the right-hand side of (2.3) so that the drag formed an energy sink for wave energy reaching low wavenumbers. The drag coefficient γ was set to 0 for $k > 3$, ensuring that only a few low modes were effected by drag. Consequently, the inertial range that develops in the wavenumber interval $3 < k < 640$ was completely free of dissipative effects.

Numerical integrations were started from zero initial conditions, i.e. at $t = 0$ we set $u = v = h = 0$, and the high wavenumber forcing was the only source of waves for the system. Numerical integrations beginning from a state of rest were seen to be required to go up to $t \sim 15\,000$ for the flow to form a broad spectrum of waves in a statistical steady state. The long-time forced-dissipative equilibrated state of the system was confirmed by monitoring energy and various statistical quantities described in the following section. Once the flow was seen to reach an equilibrated state, the equations were integrated for an interval $\Delta t = 50\,000$, this being the interval during which the averaging of statistical quantities given below were computed. A further increase in the averaging time interval was not seen to change the quantities by a noticeable margin, which is why we chose $\Delta t = 50\,000$ as the averaging interval.

3. Results

As mentioned earlier, in a turbulent flow composed of inertia-gravity waves, wave action is fluxed to larger scales. Consequently, the action flux moves waves forced at high wavenumbers to low wavenumbers or larger scales. For unit rotation rate $f = 1$, figure 1(*a*) shows the action spectrum of waves in forced-dissipative equilibrium. Since the waves' dispersion relationship (2.4) prevents resonant triads, quartic resonances form the leading interaction. For a wavenumber quartet (k, k_1, k_2, k_3), we have the resonance conditions

$$k = k_1 + k_2 + k_3 \tag{3.1a}$$

and

$$\omega(k) = \pm\omega(k_1) \pm \omega(k_2) \pm \omega(k_3). \tag{3.1b}$$

Note that every wavenumber, say k_1 for example, can take positive and negative values, which is why we did not add $\pm$ in the wavenumber relationship in (3.1*a*). Solving the above resonance equations using the dispersion relationship (2.4) gives us $k_1 = -k_2$, $k_1 = -k_3$ and $k_2 = -k_3$ as the resonant curves. To examine the relevance of quartic resonances in the waves' upscale transfer, we computed the tricoherence coefficient

$$\mathscr{T}(k_1, k_2, k_3) = \frac{|\langle \hat{u}_k^* \hat{u}_{k_1} \hat{u}_{k_2} \hat{u}_{k_3} \rangle|}{\langle |\hat{u}_k| \rangle \langle |\hat{u}_{k_1}| \rangle \langle |\hat{u}_{k_2}| \rangle \langle |\hat{u}_{k_3}| \rangle}, \tag{3.2}$$

where $k = k_1 + k_2 + k_3$, $*$ denotes complex conjugate and $\langle \rangle$ denotes time averaging. The tricoherence coefficient, $0 \leqslant \mathscr{T} \leqslant 1$, is similar to the bicoherence coefficient used to examine triadic wave interactions (MacKinnon *et al.* 2013; Aubourg & Mordant 2015; Meyrand *et al.* 2018). We examined $\mathscr{T}(k_1, k_2, k_3)$ for a wide range of wavenumbers and an example visualization of the coefficient in the k_1–k_2 plane for $k_3 = 30$ is shown in figure 1(*b*). Note that the high correlation regions, which appear as bright green lines in
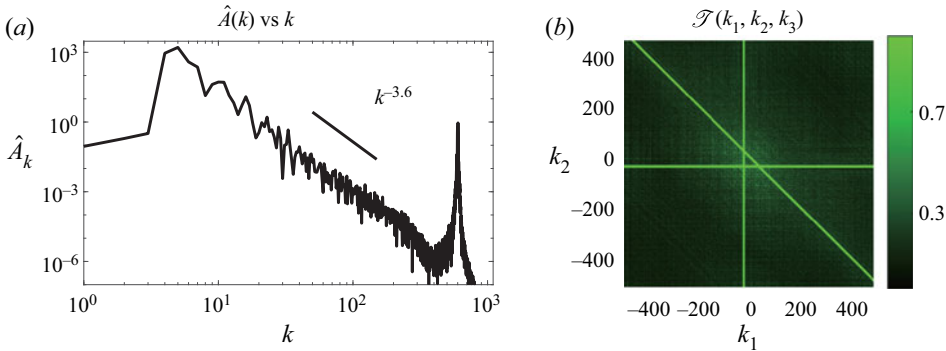
Figure 1. (*a*) Action spectrum for $f = 1$. Time-averaged spectral slope in the inertial range was seen to be -3.6. Panel (*b*) shows $\mathscr{T}(k_1, k_2, k_3)$ for $k_3 = 30$. The high correlation bright green lines are the resonant curves: $k_1 = -k_3$, $k_2 = -k_3$ and $k_1 = -k_2$.

the figure, correspond to resonant curves given by $k_1 = -k_2$, $k_1 = -30$ and $k_2 = -30$, as predicted by the resonant quartic solutions.

Despite $\mathscr{T}(k_1, k_2, k_3)$ being dominated by four wave resonances, there are signatures of near-resonant and non-resonant transfers. A reader staring carefully at figure 1(*b*) will notice that, although not as intense as the bright green lines, there are high correlation (greenish) regions located away from the bright lines; these regions being an indication of non-resonant transfers. Additionally, the exact resonance curves obtained by solving (3.1) are straight lines with zero thickness, whereas the lines in figure 1(*b*) have finite thickness and is a signature of near-resonant exchanges.

Overall, the behaviour seen in figure 1(*b*) was seen to be generic for wavenumbers throughout the system. Despite signatures of non-resonant and near-resonant transfers being persistent, high correlation regions in $\mathscr{T}(k_1, k_2, k_3)$ generically coincide with exact four wave resonance curves, indicating that quartic resonant interactions are the predominant mechanism responsible for the upscale transfer of waves.

3.1. *Non-local transfer of wave action*

The above discussion of resonant modes indicates that wavenumbers of disparate lengths can interact and influence each other. For instance, a set of wavenumbers consisting of wavenumbers that are a decade apart, $(k, k_1, k_2, k_3) = (30, 300, -300, 30)$, interact since this set lies on the resonant manifold $k_1 = -k_2$. In general, the resonant manifolds $k_1 = -k_2$, $k_1 = -k_3$ and $k_2 = -k_3$ are all composed of a broad set of non-local wavenumbers, indicating that the upscale transfer of waves in RSWE involves the interaction of non-local modes.

Of course, non-local wavenumbers being involved in the turbulent transfer term does not necessarily imply that the transfer itself is non-local. For instance, as is the case in three-dimensional homogeneous isotropic turbulence (3-D HIT), the turbulent transfer can be local although non-local modes participate in the transfer. To place these ideas on a firm foundation, especially for the sake of readers unfamiliar with local and non-local turbulent transfers, we will briefly visit these well established notions in 3-D HIT before dwelling into the locality of transfers in RSWE.

In 3-D HIT energy is fluxed downscale via triadic interactions. The energy equation in spectral space reads

$$\frac{\partial \hat{E}_k}{\partial t} = \sum_{k_1} \sum_{k_2} S_E(k|k_1, k_2) = \sum_{k_1} T_E(k|k_1) = R_E(k). \tag{3.3}$$

In the above equation, $S_E(k|k_1, k_2)$ is the triadic nonlinear term in spectral space responsible for all energy transfer between wavenumbers k_1, k_2 and k subject to the triadic constraint $k = k_1 + k_2$. Summing $S_E(k|k_1, k_2)$ over k_2 gives us the transfer function $T_E(k|k_1)$, which captures transfers between wavenumbers k and k_1. Finally, summing over k_1 gives us the net energy transfer at a specific wavenumber, $R_E(k)$.

Locality of transfers in turbulent flows is quantified based on $T_E(k|k_1)$ in (3.3), which captures the transfers between wavenumbers k and k_1. Since $S_E(k|k_1, k_2)$ was summed over k_2 to obtain $T_E(k|k_1)$, it is clear that non-local triads contribute towards transfer of energy across scales. For instance, the lengths of wavenumbers k and k_1 can be comparable, while k_2 can be of really small length resulting in $k_2 \ll k \sim k_1$. Such widely separated or non-local wavenumbers can affect the transfer. Although non-local wavenumbers participate in the transfer, conventionally in hydrodynamic turbulence a transfer is identified as local if most of the transfer term $T_E(k|k_1)$ is concentrated on wavenumbers $k \sim k_1$. This means that the transfer at a specific wavenumber k is due to wavenumbers k_1 in the neighbourhood of k such that $k/k_1 \sim 1$. On the other hand, if wavenumbers k_1 significantly away from k such that $k/k_1 \gg 1$ or $k/k_1 \ll 1$ contribute towards the transfer at wavenumber k, it is termed a non-local transfer (Brasseur & Wei 1994; Lesieur 2008).

A broad set of studies focusing on 3-D HIT have revealed that although non-local wavenumbers play a role in the transfer, the energy transfer from large to small scales is local (Domaradzki & Rogallo 1990; Yeung & Brasseur 1991; Ohkitani & Kida 1992; Waleffe 1992; Zhou 1993; Brasseur & Wei 1994; Domaradzki & Carati 2007; Eyink & Aluie 2009; Cardesa, Vela-Martin & Jimenez 2017). Figure 2(a) shows an example plot of time averaged $T_E(k|k_1)$ normalized by the maximum absolute value of the transfer term from a 2048^3 resolution 3-D HIT numerical integration with k being chosen to be in the middle of the inertial range. The numerical set-up was similar to that used in Thomas & Daniel (2020, 2021), except that the incompressible Navier–Stokes equations were integrated instead of the Boussinesq equations integrated in Thomas & Daniel (2020, 2021). The flow was stochastically forced at low wavenumbers and was dissipated at small scales by hyperdissipation. We skip further technical details here primarily since figure 2(a) is a popular result that has been persistently observed in a wide range of studies exploring the locality of turbulent transfers in 3-D HIT (see similar figures in Domaradzki & Rogallo (1990) and Yeung & Brasseur (1991) for example). For a reader unfamiliar with the locality of transfers in HIT, it is crucial to note that the transfer function $T(k|k_1)$ is localized around $k \sim k_1$. Observe how the function is negative for $k < k_1$ and positive for $k > k_1$, implying that energy is being transferred locally from left to right. The energy transfer at a specific wavenumber k is therefore exclusively due to wavenumbers k_1 in the neighbourhood of k. Figure 2(a) therefore summarizes a well-established feature of the turbulent energy cascade in 3-D HIT: despite non-local wavenumbers being involved in the transfer term, the turbulent downscale transfer of energy is local.

Although 3-D HIT has no straightforward connections to the present study focusing on RSWE, the above discussion of locality of transfers in 3-D HIT was to introduce an unfamiliar reader to key technical details of the locality of turbulent transfers. Given the understanding summarized in the above passages on the locality of transfers, we will now
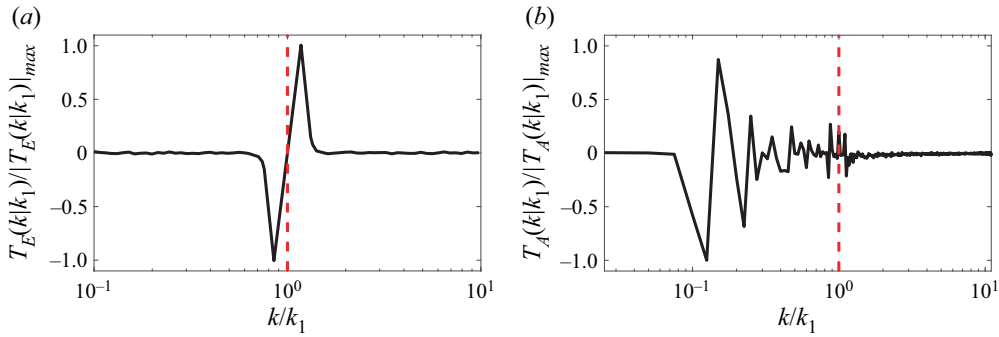
961 A2-8

Figure 2. Transfer terms normalized by their absolute maximum for (*a*) 3-D HIT and (*b*) RSWE. The transfer terms were time averaged to remove fast-in-time high frequency fluctuations.

examine the locality of transfers in RSWE. To get a handle on wave action transfer in RSWE, we take the Fourier transform of (2.3) and manipulate to form the wave action equation in spectral space as

$$\frac{\partial \hat{A}_k}{\partial t} = \sum_{k_1} T_A(k|k_1).$$ (3.4)

Above, $T_A(k|k_1)$ captures action transfer between wavenumbers k and k_1 and summing over k_1 gives us the net action transfer at a specific wavenumber k. Figure 2(*b*) shows the time-averaged transfer function $T_A(k|k_1)$ normalized by the absolute maximum of the transfer term for RSWE with $k = 50$, a wavenumber in the middle of the inertial range as can be seen from figure 1(*a*). Observe that the transfer term is highly non-local: the transfer has little contribution from the local neighbourhood of $k \sim k_1$ and the major fraction of the contribution to the transfer term is from wavenumbers k_1 located significantly away from k. Although the quantitative details in figure 2(*b*) are for a specific wavenumber $k = 50$, the qualitative nature of the figure was seen to be generic for wavenumbers across the inertial range, i.e. extremely disparate wavenumbers k_1 are responsible for the transfer at a wavenumber k. The upscale transfer of inertia-gravity waves is therefore a non-local turbulent transfer involving the action transfer between extremely disparate scales or wavenumbers. Interestingly, examples of highly non-local transfers in dispersive wave turbulence have been observed in the past (see, for example, discussions in Cai *et al.* 1999), non-local transfers being a feature that distinguishes scale-local strongly nonlinear transfers in 3-D HIT from resonance-dominated transfers in weakly nonlinear wave turbulence such as the one explored in our present study.

3.2. *Intermittency in upscale transfers*

Our findings so far point out that upscale wave transfers based on resonant four wave interactions is robustly seen in RSWE, as predicted by wave turbulence theory. Despite observing the upscale transfers as per the theoretical prediction, we found features of the flow such as intermittency and non-Gaussian statistics, indicating departures from assumptions used in classical wave turbulence theory. Intermittency of turbulent transfers is a persistent feature seen in turbulent wavy flows (Falcon *et al.* 2007*a*,*b*, 2008, 2010; Falcon & Mordant 2022) and we found strong features of intermittency in our solutions and transfer across scales. On tracking different variables associated with the turbulent

transfer, the action flux was seen to be an obvious indicator of intermittent transfers. Summing (3.4) from the lowest wavenumber to an arbitrary wavenumber gives us the time evolution equation of wave action contained in the wavenumber band $[0, k]$ as

$$\frac{\mathrm{d}}{\mathrm{d}t} \left(\sum_{n=0}^{n=k} \hat{A}_n \right) = \Pi_k, \tag{3.5}$$

where Π_k is the flux of wave action. Since action is being transferred from smaller scales to larger scales, on average the flux Π_k should be positive. Figure 3(*a*) shows the probability density function (PDF) of flux for an example wavenumber $k = 50$, with the dashed red line showing the mean of the PDF. Note that the flux PDF is almost symmetric, with a slight skewness to the right. The mean of the action flux is positive, indicating that waves are on average getting transferred upscale. To highlight a specific detail of the transfer, figure 3(*b*) shows a short-time series of the action flux. Observe that the flux oscillates between positive and negative values with intermittent positive jumps: a notable positive jump is seen at $t = 24.5$ in figure 3(*b*). The upscale transfer of waves is associated with such localized-in-time positive jumps in the action flux, these intermittent events being the cause of the slightly skewed PDF with a positive mean shown in figure 3(*a*). Although these details correspond to $k = 50$, the intermittency of flux was observed generically for wavenumbers in the inertial range.

The intermittent upscale transfers described above were seen to directly affect the inertial range of waves. Specifically, the slope of the waves' spectrum was seen to change with time, with the spectrum becoming shallower following the positive bursts in flux. Figure 3(*c*) shows the slope of the spectrum, $n(t)$, as a function of time in the same time interval as figure 3(*b*). The time-averaged slope of the spectrum is -3.6 and is marked by the dashed red line, this being the slope marked in figure 1(*a*). On comparing figures 3(*b*) and 3(*c*), it can be seen that the positive jump in flux at $t = 24.5$ is followed by the highest slope in the time interval shown. On examining different windows of time series of the waves' spectral dynamics, this was seen to be a generic feature: intermittent positive jumps in flux are followed by the waves' spectrum becoming shallower, indicating an energization of waves across scales in the waves' spectrum.

The intermittent dynamics of waves in spectral space described above corresponds to similar changes in physical space. A common tool to visualize intermittency is to track the changes in the PDF of velocity differences $\delta u(\tau) = u(t + \tau) - u(t)$ (Frisch 1995). Specifically, PDFs of velocity increments, δu, deform with time lag τ. At short-time lags, δu has fat tails compared with a Gaussian distribution, while at longer τ the PDF approaches a Gaussian distribution. This behaviour of PDFs of increments in velocity deforming with time lag is a signature of intermittency and has been reported multiple times in surface wave turbulent flows (Falcon *et al.* 2007*b*, 2010). Figure 3(*d*) shows the PDFs of the δu for $\tau = 0.2$ and $\tau = 5$. The deformation of the PDF from a fat tailed distribution at lower τ to approaching a Gaussian distribution for larger τ is a direct reflection of intermittent turbulent transfers.

Tracking the flux and the inertial range behaviour of waves, we found that the intermittent events started at small scales and then propagated to larger scales. This information is reflected in figure 3(*d*), which indicates that intermittency is highest at small scales and lowest at large scales. The intermittent positive bursts in flux transfers waves upscale, eventually affecting domain-scale waves. On carefully monitoring the wave fields over time, we consistently observed that the intermittent positive jumps in flux were followed by higher energy level domain-scale waves. An illustration of this is shown in
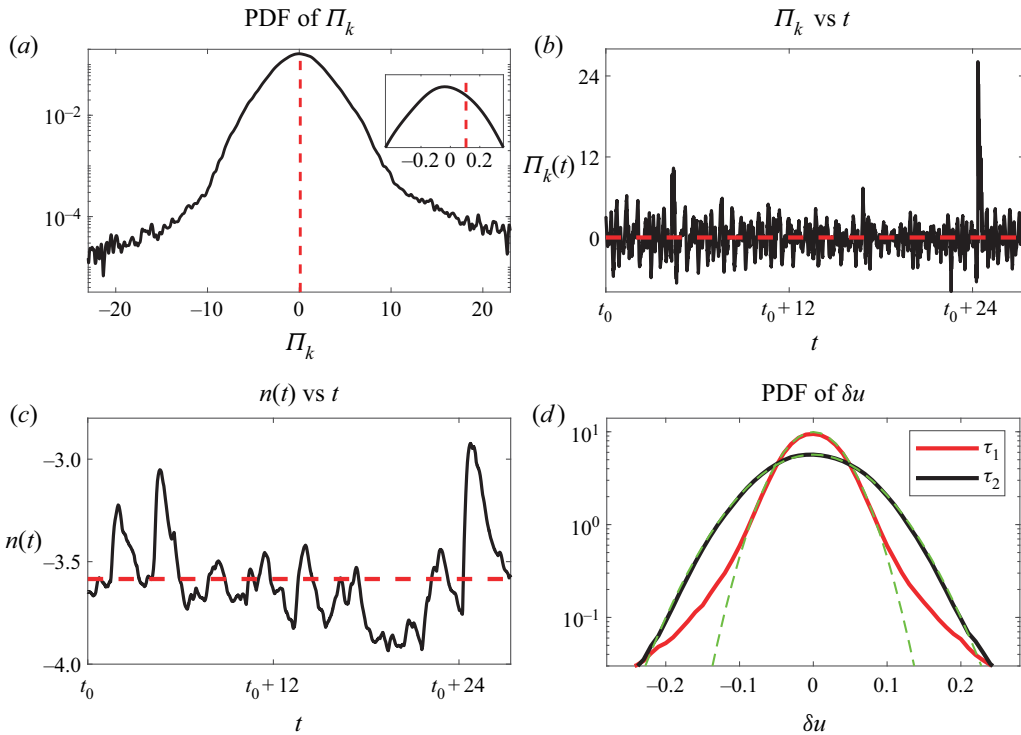
Figure 3. Panel (*a*) shows the PDF of action flux Π_k for $k = 50$ while the inset shows a smaller part of the PDF. The mean of the PDF is shown by the dashed red vertical line. The PDF has skewness 0.19 and kurtosis 5.6. Panel (*b*) shows a short-time series of the action flux Π_k for $k = 50$ and t_0 is a reference time instant. The mean of the time series is indicated by the dashed red horizontal line. Observe that the flux time series shows a strong positive jump at $t = t_0 + 24.5$. Panel (*c*) shows a short-time series of the slope of the inertial range. Note that the slope takes up a high value, i.e. becomes shallower, following the positive burst in flux at $t = t_0 + 24.5$. The mean slope, $n = -3.6$, is indicated by the horizontal dashed red line and is marked by the straight black line in figure 1(*a*). Panel (*d*) shows the PDF of the velocity increment $\delta u = u(t + \tau) - u(t)$ for $\tau_1 = 0.2$ and $\tau_2 = 5$.

figure 4, the four panels corresponding to four different times in the time interval shown in figures 3(*b*) and 3(*c*). Note that the wave field's amplitude is highest in figure 4(*c*), which corresponds to the flux burst at $t = t_0 + 24.5$ seen in figure 3(*b*). Away from the flux burst point, the amplitude of the wave field is relatively small, as can be seen in panels 4(*a*), 4(*b*) and 4(*d*). On examining the physical structure of waves across long-time intervals, we observed that the intermittent positive burst in the waves' flux goes hand in hand with an amplification of the waves' strength in physical space, i.e. high wave amplitudes were in general positively correlated with flux bursts.

3.3. *Departure from Gaussian statistics*

Gaussian statistics for the flow fields and a random distribution of wave phases are typical assumptions used in wave turbulence theory (Zakharov *et al.* 1992; Nazarenko 2011). Therefore, a random uncorrelated distribution for the phases $\arg(\hat{u}_k)$, $\arg(\hat{v}_k)$, $\arg(\hat{h}_k)$ is expected in wave turbulent flows. We examined the statistics of the flow variables from our solutions and figure 5(*a*) shows the distribution of the phase, $\arg(\hat{u}_k) \in [-\pi, \pi]$, for three wavenumbers, $(k_1, k_2, k_3) = (10, 50, 300)$. The phases were averaged over a long interval
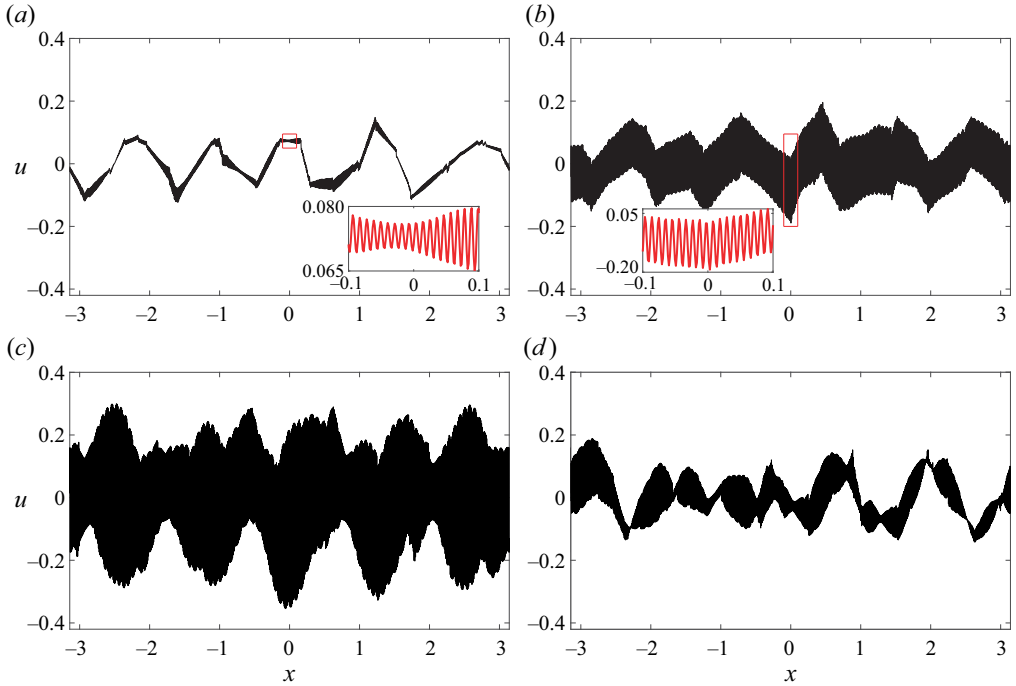
Figure 4. The physical structure of u at four different times in the neighbourhood of the positive jump in flux at $t = t_0 + 24.5$ seen in figure 3(b). Specifically, u is shown at (a) $t = t_0 + 23.9$, (b) $t = t_0 + 24.2$, (c) $t = t_0 + 24.5$, (d) $t = t_0 + 24.7$. The insets in panels (a,b) show a zoomed-in view of the red rectangular regions in the main figures. The highest amplitude waves, seen in panel (c) above, correspond to the flux burst at $t = t_0 + 24.5$ in figure 3(b).
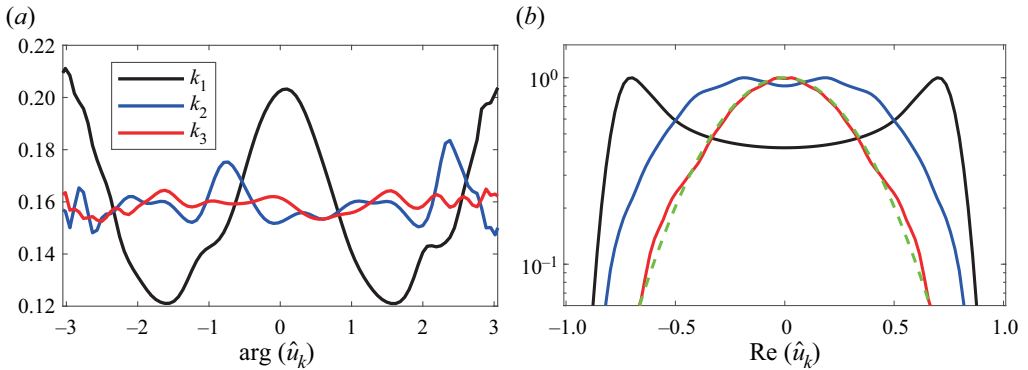

Figure 5. (a) The PDF of phases of $\hat{u}_k$ for three different wavenumbers $(k_1, k_2, k_3) = (10, 50, 300)$. (b) The PDF of the real part of $\hat{u}_k$ for the same three wavenumbers. A Gaussian curve is shown by a dashed green line for reference.

such that the distribution saturated to that shown in the figure. As seen in the figure, the phases are less uniform at low wavenumbers and approach a uniform distribution at high k. A similar behaviour is seen for the PDF of $\mathrm{Re}(\hat{u}_k)$, the real part of $\hat{u}_k$, shown in figure 5(b). Observe that the lowest wavenumber shows a bimodal distribution that transitions gradually into a Gaussian distribution for the highest wavenumber.

961 A2-12

It is intriguing that although intermittency was seen to propagate from small scales to large scales, as discussed in § 3.2, the departure of wave phase and amplitude from idealized Gaussian distribution that is typically assumed in wave turbulence theory is highest at large scales. Furthermore, it is noteworthy that large scales carrying most of the energy departing from Gaussian distribution is a feature that has been observed in multiple past studies, especially studies focusing on waves undergoing a forward flux (Yokoyama 2004; Chibbaro & Josserand 2016). Given these past results, we speculate that our finding of the departure from Gaussian statistics at large scales might not be specific to the upscale transfer of waves. The large scales carrying most of the total energy in the system departing from idealized Gaussian assumptions could be a more generic result applicable to arbitrary turbulent wavy systems, independent of whether the waves undergo forward or inverse flux.

3.4. *Effect of increasing rotation rate*

On increasing the rotation rate we observed that upscale transfers were weakened and it took a much longer time to form broad spectrum waves in forced-dissipative equilibrium. As follows from the dispersion relationship (2.4), for a fixed wavenumber, the wave frequency increases with f and the group velocity of waves $c_g = k/\sqrt{f^2 + k^2}$ decreases with increasing f, making propagation of wave packets slower. Furthermore, increasing f reduces the scale-specific Rossby number, $Ro_k = kU_k/f$, where U_k is the flow velocity magnitude at wavenumber k. The reduction in Rossby number and wave group velocity weakens the nonlinear interactions, making turbulent transfers slow and inefficient at higher rotation rates. A qualitatively similar effect was seen in Farge & Sadourny (1989) while investigating wave-vortex dynamics in two-dimensional RSWE. Farge & Sadourny found that high rotation rates led to a 'freezing' of the turbulent transfers in their relatively short-time interval numerical integrations. In our investigation, due to weakened upscale transfers, we had to numerically integrate the equations for much longer times. With weakened nonlinear interactions and slower turbulent transfers, we found the wave energy levels to slightly increase at an intermediate wavenumber, rather than the lowest wavenumbers, resulting in slightly steeper wave spectra at higher f.

The features mentioned above can be seen in the waves' spectra for different f in figure 6: observe that the energy content at low wavenumbers, $k \lesssim 15$, is less for $f = 4$ and $f = 2$ when compared with the $f = 1$ case, and the spectra are slightly steeper at higher f. Apart from reduced upscale transfers and other minor quantitative changes, all the qualitative features described earlier for $f = 1$, i.e. resonant quartics playing the major role in upscale transfers, the non-local nature of the transfer, intermittency of the transfer observed in the inertial range and in the physical structure of the waves, and low wavenumbers departing the most from idealized Gaussian assumptions, were seen to be similar at higher rotation rates. We therefore omit further figures on turbulent transfers at high rotation rates and end on the note that upscale transfers are retarded on increasing the rotation rate.

3.5. *Comparison with predictions based on wave turbulence theory*

As discussed earlier, wave turbulence theory has been applied to RSWE to obtain predictions for the turbulent spectra corresponding to the waves' upscale transfer. Based on theoretical calculations, Falkovich (1992) and Falkovich & Medvedev (1992) found that the waves' action spectrum was between $k^{-13/3} \approx k^{-4.3}$ and $k^{-8/3} \approx k^{-2.7}$ for different limits of rotation and dispersion. Following this, Glazman (1996) extended the theoretical calculations by including higher-order wave interactions and obtained slightly refined
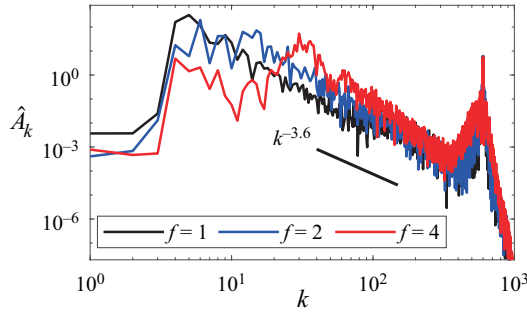
Figure 6. Action spectra for different f. The black curve is the same spectrum shown in figure 1. Note that the energy content at low wavenumbers decreases at higher f.

estimates for the waves' spectrum. It is noteworthy that all the spectra we obtained by numerical integration of the governing equations lie between $k^{-4.3}$ and $k^{-2.7}$ (see figure 6), which is the range of spectra predicted based on wave turbulence theoretical calculations by Falkovich (1992) and Falkovich & Medvedev (1992).

Despite the waves' spectra we obtained being within the interval predicted by previous theoretical estimates, multiple caveats must be emphasized here. In wave turbulence theoretical formalism, the waves' spectrum emerges as an equilibrium solution, that is, the exponent n of the spectrum k^{-n} is a fixed number. However, as explained earlier, the waves' upscale transfers are intermittent and not steady, leading to a waves' spectrum that fluctuates significantly over time (recall figure 3c). Additionally, Gaussian statistics and random phases for wave fields are central assumptions in wave turbulence theory, these conditions also not being satisfied by the solution of the equations we found (recall figure 5). To obtain improved estimates for the waves' spectrum, Glazman (1996) included higher-order wave interaction terms and assumed the locality of transfers in spectral space, a feature that was seen to be violated in upscale transfers in RSWE, as explained in connection to figure 2.

The above discussion brings out the challenges in comparing theoretical wave turbulence based predictions with numerical results obtained in the present work. Much of the idealized assumptions used in wave turbulence theory are not satisfied by the solutions of the governing equations we obtained via direct numerical integrations. Not surprisingly, similar departures have been reported in numerical and laboratory experiments exploring turbulent dynamics of waves in different set-ups (Yokoyama 2004; Falcon *et al.* 2007a,b; Korotkevitch 2008; Falcon *et al.* 2008, 2010; Chibbaro & Josserand 2016). Our results therefore add to the growing list of evidence of wave turbulence theoretical predictions departing from numerical and experimental results on weakly nonlinear turbulent wave-dominated flows. These findings in general stress the need to improve the theoretical foundations of wave turbulence theory, so as to obtain better theoretical predictions that align with numerical and experimental results.

4. Summary and perspectives

In this paper we explored the upscale transfer of inertia-gravity waves in one-dimensional RSWE. The dispersion relationship of inertia-gravity waves in RSWE prohibits resonant triads, leading to a second integral conserved quantity in addition to energy: wave action. Consequently, in a turbulent flow consisting of inertia-gravity waves, wave energy is transferred to small scales while wave action gets transferred to larger scales. Although theoretical calculations based on wave turbulence theory have predicted the possibility

of upscale wave transfers three decades back, no study has confirmed the phenomenon by integrating the governing equations. The lack of an investigation exploring the details of the waves' upscale turbulent transfer inspired our present work, where we used direct numerical integration of the equations to study the upscale transfer of waves.

Our study revealed that resonant four wave interactions were primarily responsible for the waves' upscale transfer. Non-local wavenumbers were involved in the turbulent transfer and the transfer itself was non-local, i.e. wave action was exchanged between extremely disparate scales. Additionally, the turbulent transfer was not continuous in time, rather upscale transfers took place via localized-in-time bursts of the action flux that moved waves on average to larger scales. These intermittent bursts in action flux went hand in hand with the shallower waves' spectra and energetic high amplitude wave fields in physical space. The intermittency of upscale wave transfers were therefore noticeable in spectral space and physical space. Finally, the statistics of the wave field were seen to depart from Gaussian at larger scales, while smaller scales exhibited Gaussian behaviour. This shows a departure from typical assumptions used in wave turbulence theory, where the wave phases, for example, are assumed to be random and uncorrelated with Gaussian dynamics.

Contrary to vortical turbulent dynamics that requires at least two physical dimensions, wave turbulence can be realized in a single dimension. This attractive feature has inspired the development and integration of multiple one-dimensional mathematical models exploring turbulent dynamics of a broad spectrum of waves (Majda *et al.* 1997; Cai *et al.* 2001; Zakharov *et al.* 2004). Similar inspirations have led to studies exploring wave turbulent-like dynamics in one-dimensional Burgers equation (see discussions and references in Murray & Bustamante 2018). The key here is that long-time high accuracy numerical integration is possible for one-dimensional models with affordable computational resources, allowing us to dwell into details of turbulent transfers that are not straightforward with higher-dimensional models. On a relative comparison, one-dimensional RSWE is a more realistic physical model than previously mentioned adhoc toy models and is a popular work horse in the geophysical fluid dynamics community. With the forward flux and multiple related dynamics of this model being explored in the past, our findings point out that the model also captures the rich non-trivial dynamics associated with the inverse flux of waves. Consequently, one-dimensional RSWE could be used as a slightly more realistic model than pre-existing adhoc models for future studies focusing on aspects related to the upscale transfer of dispersive waves.

Despite capturing the inverse flux of inertia-gravity waves, a notable feature observed in the present study was that the upscale transfers were generically slow, with $t \sim O(10\,000)$ being the typical time scale to obtain a broad spectrum of waves in forced-dissipative equilibrium. Figure 7 shows, for example, the different stages of the waves' spectra until it reaches an equilibrated state. Given the slow nature of the process, it is unclear how noticeable the upscale transfer of waves would be in realistic atmospheric and oceanic flows where many other processes operate on much faster time scales. However, although the waves' spectrum takes a long time to reach equilibrium, intermittent and bursty upscale transfers detailed with figures 3 and 4 were seen during the intermediate stages shown in figure 7, before reaching equilibrium. Therefore, even on relatively short-time scales, wave activity at small scales can intermittently propagate to larger scales and accumulate at the inertial frequency, this being the ubiquitous low frequency peak in the oceanic wave spectrum (Garrett 2001; Alford *et al.* 2016). Direct forcing by wind and spontaneous emission by vortical flows are considered to be the prominent mechanisms responsible for the inertial peak (D'Asaro 1985; Vanneste 2013). Notably, there is no
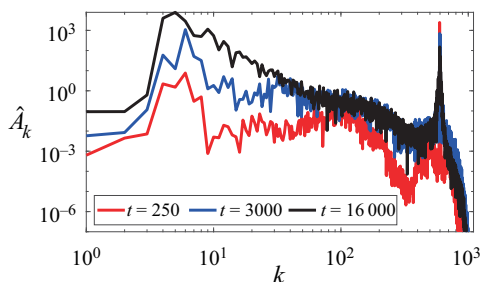
Figure 7. Action spectra for $f = 1$ case at three different times. The broad spectrum of waves reaches an equilibrated state around $t = 15\,000$.

obvious explanation for near-inertial waves in regions with negligible wind forcing and vortical flow. Therefore, the inverse flux of inertia-gravity waves could play a role in energizing an inertial frequency peak in such regions, despite the slow nature of the waves' upscale transfers.

Turbulent transfers in coastal oceanographic regions is another area where upscale wave transfers could have potential relevance. Multiple observations have indicated upscale transfers in shallow oceanographic regions near the coast (Soh & Kim 2018; Yoo, Kim & Kim 2018; Elgar & Raubenheimer 2020). However, quite often the inverse flux is attributed to the vortical mode alone and the waves' contribution is not critically evaluated. In other words, although upscale transfers are observed in coastal areas, there has been no dedicated efforts to separate the transfers due to waves alone from the vortical transfers. As mentioned earlier, given the slow nature of the upscale transfer of waves, further studies in realistic settings are needed to compare the relative rates of the upscale transfer of vortices and waves so as to examine whether the inverse flux of waves in coastal regions can form a non-negligible contribution to the net inverse flux of the flow.

Finally, the results of the present work point towards interesting ramifications for long term dynamics of RSWE, specifically in two dimensions. Given that our study confirms the inverse flux of inertia-gravity waves in one dimension, we anticipate the same phenomenon in two dimensions. Furthermore, the vortical mode that was ignored in the present study evolves and fluxes energy upscale in two dimensions. This means that both waves and the vortical mode can exhibit upscale transfers in two dimensions, challenging a well-established paradigm in geophysical fluid dynamics. In geophysical flows waves typically dissipate at small viscous scales due to downscale energy transfer while the vortical mode transfers energy upscale and undergoes negligible dissipation. As a result of waves disappearing from the system by small-scale dissipation, the long-time state of geophysical flows is assumed to be composed primarily of the vortical mode and negligible waves, this process being an example of turbulent geostrophic adjustment (Bartello 1995; Reznik 2015).

In light of the present study, it is natural to speculate that the upscale transfer of waves would result in a non-negligible amount of waves at large scales, along with the vortical mode. Consequently, contrary to the conventional hypothesis based on geostrophic adjustment, the long-time limit of RSWE in two dimensions could be a mixture of fast inertia-gravity waves alongside slowly evolving vortices. Surprisingly, almost four decades back Warn (1986) used equilibrium statistical mechanics machinery to predict that the long-time state of RSWE would be rich with fast inertia-gravity waves (also see the generalization of Warn's result by Renaud, Venaille & Bouchet 2016). This unusual result of Warn and the details of the process remain untested to date, primarily due to the lack of

extremely long-time numerical integration results of two-dimensional RSWE with waves and vortical modes. Past studies that have numerically integrated two-dimensional RSWE have focused primarily on the dynamics of the vortical mode, wave-vortex interactions on short-time scales and the forward flux of waves and shock formation (Farge & Sadourny 1989; Polvani *et al.* 1994; Yuan & Hamilton 1994; Remmel & Smith 2009; Ward & Dewar 2010; Lahaye & Zeitlin 2012), contributing to the lack of an understanding of the long-time state of RSWE. Given the upscale wave transfers in RSWE, although specific details might differ, it is tempting to think that Warn's conclusion might have some significance in the long-time limit of RSWE.

Of course, investigating the above-mentioned realistic processes and the long-time limit of RSWE mentioned in the previous paragraph will require high-resolution long-time direct numerical integration of the two-dimensional RSWE by including the vortical mode. As mentioned earlier, in the present study the one-dimensional nature of the equations allowed us to integrate the equations for really long-time scales with high precision numerical accuracy. A typical time scale for obtaining forced-dissipative equilibrium flows and collecting all the relevant statistical quantities in our one-dimensional study was $t \sim O(50\,000)$ and it is extremely challenging to integrate the two-dimensional RSWE for such long times. Consequently, decoding turbulent upscale transfers in two-dimensional RSWE remains to be an exceptionally challenging undertaking. In conclusion, although many different facets of RSWE have been explored in the past (Zeitlin 2018), the turbulent long-time state of RSWE still remains an open question that requires a detailed investigation.

Declaration of interests. The authors report no conflict of interest.

Author ORCIDs.

Jim Thomas https://orcid.org/0000-0002-5431-1619.

Appendix. Confirmation that linear waves dominate the flow

All the numerical integrations of (2.3) with $\epsilon \ll 1$ were performed with wave forcing alone, excluding the vortical mode. Here we present details of the flow structure to confirm that the flow was dominated by linear inertia-gravity waves alone.

As mentioned in § 2, the quadratic and cubic energies given by (2.5) and (2.6) are indistinguishable in the weakly nonlinear regime. In all our numerical integrations, the quadratic energy E was seen to approximate the cubic energy E^ϵ very well. Furthermore, the quadratic and cubic energies were seen to agree well pointwise in physical and spectral space. A specific example is shown in figure 8(*a*) for $f = 1$; note that the red and black curves denoting the spectrum of quadratic and cubic energies overlap, indicating that the quadratic energy approximates the cubic energy very well.

The linear modes of RSWE comprise of inertia-gravity waves and a geostrophically balanced vortical mode. In our forced-dissipative simulations, although we ensured that the stochastic forcing scheme injected only waves and no vortical mode, nonlinear interactions generated a weak vortical field. This can be seen in figure 8(*a*), which shows the energy spectrum of the quadratic vortical energy $E_v = 1/2(u_v^2 + v_v^2 + h_v^2)$. Note that the vortical spectrum is more than eight orders of magnitude below the total energy spectrum,
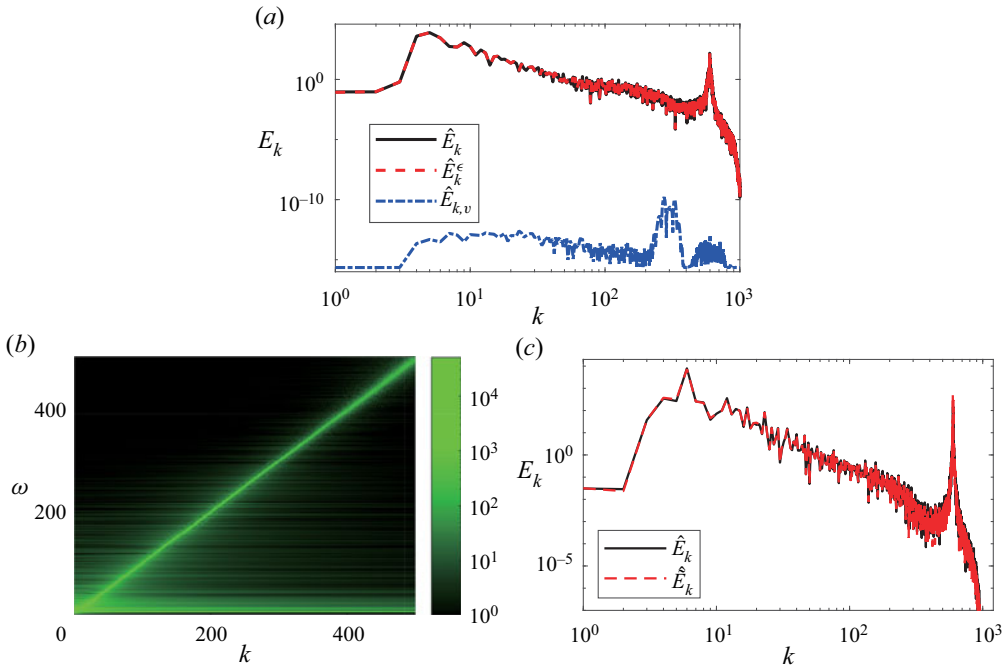
Figure 8. (*a*) A comparison between quadratic $\hat{E}_k$ (black line) and cubic $\hat{E}_k^\epsilon$ (red line) energy spectra of RSWM at a certain time instant. The low-energy vortical energy spectrum $\hat{E}_{k,v}$ is shown in blue; (*b*) $\hat{u}_k^\omega$, the frequency-wavenumber spectrum of u; (*c*) time-averaged quadratic energy spectrum $\hat{E}_k$ compared with a time-filtered energy spectrum $\hat{\tilde{E}}_k$. The quadratic energy spectrum was time averaged over the same time interval used to generate the time-filtered energy spectrum. The agreement between the two confirms that the flow is almost entirely composed of linear waves.

indicating that the vortical field is negligible in the flow and inertia-gravity waves almost entirely make up the full flow field.

Based on a numerical integration of (2.3) with $f = 1$, figure 8(*b*) shows the frequency–wavenumber spectrum of u, denoted as $\hat{u}_k^\omega$. The frequency–wavenumber spectrum, $\hat{u}_k^\omega$, was obtained by storing the time series of each wavenumber of $\hat{u}_k$ and then performing a Fourier transform to the time series to get the frequency content of $\hat{u}_k$ for each wavenumber k. Observe that the high intensity region in figure 8(*b*) aligns with the straight line $\omega = k$, which approximates the dispersion relationship of waves, $\omega = \sqrt{f^2 + k^2}$, for $k \gg f$.

In addition to the confirmation from figures 8(*a*) and 8(*b*) that linear waves dominate the flow fields, we further used a filtering approach to separate the linear wave component from the total flow fields. For the u velocity component, for example, we took $\hat{u}_k^\omega$ and, for each wavenumber k, identified a frequency band $\sqrt{f^2 + k^2} - \delta \leqslant \omega \leqslant \sqrt{f^2 + k^2} + \delta$. For pure linear waves, each wavenumber k would correspond to the exact frequency $\sqrt{f^2 + k^2}$. However, as can be seen in figure 8(*b*), weakly nonlinear interactions lead to some spread in the frequency content of the flow fields. By filtering the flow fields at each wavenumber k to the frequency window $\sqrt{f^2 + k^2} - \delta \leqslant \omega \leqslant \sqrt{f^2 + k^2} + \delta$, we obtain the part of the flow field that is closely aligned with the linear wave field. We chose δ to be $f/100$ so that the frequency window was concentrated on the dispersion relationship. After the filtering operation is performed on $\hat{u}_k^\omega$, inverse Fourier transform on ω takes the frequency-filtered

field back to the time domain. We denote such filtered fields with a tilde; for example, $\tilde{\hat{u}}_k$ is the frequency-filtered component of $\hat{u}_k$. Once all the fields are filtered, the energy spectrum of the filtered fields is given by $\tilde{\hat{E}}_k = |\tilde{\hat{u}}_k|^2 + |\tilde{\hat{v}}_k|^2 + |\tilde{\hat{h}}_k|^2$. Figure 8(*c*) shows the comparison between the unfiltered energy spectrum $|\hat{u}_k|^2 + |\hat{v}_k|^2 + |\hat{h}_k|^2$ and the filtered energy spectrum $\tilde{\hat{E}}_k$. The exceptional agreement between these two energy spectra shows that the flow fields are almost entirely linear waves, with insignificant residue.

REFERENCES

ALFORD, M.H, MACKINNON, J.A., SIMMONS, H.L. & NASH, J.D. 2016 Near-inertial internal gravity waves in the ocean. *Annu. Rev. Mar. Sci.* **8**, 95–123.

ALVELIUS, K. 1999 Random forcing of three-dimensional homogeneous turbulence. *Phys. Fluids* **11**, 1880–1889.

ANNENKOV, S.Y. & SHRIRA, V.I. 2006 Direct numerical simulation of downshift and inverse cascade for water wave turbulence. *Phys. Rev. Lett.* **96**, 204501.

AUBOURG, Q. & MORDANT, N. 2015 Nonlocal resonances in weak turbulence of gravity-capillary waves. *Phys. Rev. Lett.* **114**, 144501.

BABIN, A., MAHALOV, A. & NICOLAENKO, B. 1997 Global splitting and regularity of rotating shallow-water equations. *Eur. J. Mech.* (B*/Fluids)* **16** (1), 725–754.

BARTELLO, P. 1995 Geostrophic adjustment and inverse cascades in rotating stratified turbulence. *J. Atmos. Sci.* **52**, 4410–4428.

BOUCHUT, F., LE SOMMER, J. & ZEITLIN, V. 2004 Frontal geostrophic adjustment and nonlinear wave phenomena in one-dimensional rotating shallow water. Part 2: high-resolution numerical simulations. *J. Fluid Mech.* **514**, 35–63.

BRASSEUR, J.G. & WEI, C.-H. 1994 Interscale dynamics and local isotropy in high Reynolds number turbulence within triadic interaction. *Phys. Fluids* **6**, 842–870.

BRETHERTON, F.P. 1969 On the mean motion induced by internal gravity waves. *J. Fluid Mech.* **36**, 785–803.

CAI, D., MAJDA, A.J., MCLAUGHLIN, D.W. & TABAK, E.G. 1999 Spectral bifurcations in dispersive wave turbulence. *Proc. Natl Acad. Sci. USA* **96**, 14216–14221.

CAI, D., MAJDA, A.J., MCLAUGHLIN, D.W. & TABAK, E.G. 2001 Dispersive wave turbulence in one dimension. *Physica* D **152**, 551–572.

CARDESA, J.I., VELA-MARTIN, A. & JIMENEZ, J. 2017 The turbulent cascade in five dimensions. *Science* **357**, 782–784.

CHIBBARO, S. & JOSSERAND, C. 2016 Elastic wave turbulence and intermittency. *Phys. Rev.* E **94**, 011101.

D'ASARO, E.A. 1985 Upper ocean temperature structure, inertial currents, and Richardson numbers observed during strong meteorological forcing. *J. Phys. Oceanogr.* **15**, 943–962.

DEIKE, L., LAROCHE, C. & FALCON, E. 2011 Experimental study of the inverse cascade in gravity wave turbulence. *Europhys. Lett.* **96**, 34004.

DOMARADZKI, J.A. & CARATI, D. 2007 An analysis of the energy transfer and the locality of nonlinear interactions in turbulence. *Phys. Fluids* **19**, 085112.

DOMARADZKI, J.A. & ROGALLO, R.S. 1990 Local energy transfer and nonlocal interactions in homogeneous, isotropic turbulence. *Phys. Fluids* A **2**, 413–426.

DONG, W., BÜHLER, O. & SMITH, K.S. 2020 Frequency diffusion of waves by unsteady flows. *J. Fluid Mech.* **905**, R3.

ELGAR, S. & RAUBENHEIMER, B. 2020 Field evidence of inverse energy cascades in the surfzone. *J. Phys. Oceanogr.* **50**, 2315–2321.

EYINK, G.L. & ALUIE, H. 2009 Localness of energy cascade in hydrodynamic turbulence. I. Smooth coarse graining. *Phys. Fluids* **21**, 115107.

FALCON, E., AUMAITRE, S., FALCON, C., LAROCHE, C. & FAUVE, S. 2008 Fluctuations of energy flux in wave turbulence. *Phys. Rev. Lett.* **100**, 064503.

FALCON, E., FAUVE, S. & LAROCHE, C. 2007*a* Observation of intermittency in wave turbulence. *Phys. Rev. Lett.* **15**, 154501.

FALCON, E., LAROCHE, C. & FAUVE, S. 2007*b* Observation of gravity-capillary wave turbulence. *Phys. Rev. Lett.* **98**, 094503.

FALCON, E., MICHEL, G., PRABHUDESAI, G., CAZAUBIEL, A., BERHANU, M., MORDANT, N., AUMAITRE, S. & BONNEFOY, F. 2020 Saturation of the inverse cascade in surface gravity-wave turbulence. *Phys. Rev. Lett.* **125**, 134501.

FALCON, E. & MORDANT, N. 2022 Experiments in surface gravity-capillary wave turbulence. *Annu. Rev. Fluid Mech.* **54**, 1–25.

FALCON, E., ROUX, S.G. & LAROCHE, C. 2010 On the origin of intermittency in wave turbulence. *Europhys. Lett.* **90**, 34005.

FALKOVICH, G.E. 1992 Inverse cascade and wave condensate in mesoscale atmospheric turbulence. *Phys. Rev. Lett.* **69**, 3173–3176.

FALKOVICH, G.E. & MEDVEDEV, S.B. 1992 Kolmogorov-like spectrum for turbulence of inertial-gravity waves. *Europhys. Lett.* **19**, 279–284.

FARGE, M. & SADOURNY, R. 1989 Wave-vortex dynamics in rotating shallow water. *J. Fluid Mech.* **206**, 433–462.

FRANCOIS, N., XIA, H., PUNZMANN, H., RAMSDEN, S. & SHATS, M. 2014 Three-dimensional fluid motion in Faraday waves: creation of vorticity and generation of two-dimensional turbulence. *Phys. Rev.* X **4**, 021021.

FRISCH, U. 1995 *Turbulence: The Legacy of A. N. Kolmogorov*. Cambridge University Press.

GARRETT, C. 2001 What is the "near-inertial" band and why is it different from the rest of the internal wave spectrum? *J. Phys. Oceanogr.* **31**, 962–971.

GARRETT, C. & KUNZE, E. 2007 Internal tide generation in the deep ocean. *Annu. Rev. Fluid Mech.* **39**, 57–87.

GLAZMAN, R.E. 1996 Spectra of baroclinic inertia-gravity wave turbulence. *J. Phys. Oceanogr.* **26**, 1256–1265.

KOROTKEVITCH, A.O. 2008 Simultaneous numerical simulation of direct and inverse cascades in wave turbulence. *Phys. Rev. Lett.* **101**, 074501.

KUO, A. & POLVANI, L.M. 1997 Time-dependent fully nonlinear geostrophic adjustment. *J. Phys. Oceanogr.* **27**, 1614–1634.

KUO, A. & POLVANI, L.M. 1999 Wave-vortex interactions in rotating shallow water. Part I. One space dimension. *J. Fluid Mech.* **394**, 1–27.

LAHAYE, N. & ZEITLIN, V. 2012 Decaying vortex and wave turbulence in rotating shallow water model, as follows from high-resolution direct numerical simulations. *Phys. Fluids* **24**, 115106.

LESIEUR, M. 2008 *Turbulence in Fluids*, Fluid Mechanics and its Applications, vol. 84, 4th edn. Springer.

MACKINNON, J., ALFORD, M.H., SUN, O., PINKEL, R., ZHAO, Z. & KLYMAK, J. 2013 Parametric subharmonic instability of the internal tide at 29°N. *J. Phys. Oceanogr.* **43**, 17–28.

MAJDA, A.J. 2002 *Introduction to Partial Differential Equations and Waves for the Atmosphere and Ocean-Courant Lecture Notes, Bd. 9*. American Mathematical Society.

MAJDA, A.J., MCLAUGHLIN, D.W. & TABAK, E.G. 1997 A one-dimensional model for dispersive wave turbulence. *J. Nonlinear Sci.* **6**, 9–44.

MEYRAND, R., KIYANI, K.H., GURCAN, O.D. & GALTIER, S. 2018 Coexistence of weak and strong wave turbulence in incompressible Hall magnetohydrodynamics. *Phys. Rev.* X **8**, 031066.

MOUM, J.N. 2021 Variations in ocean mixing from seconds to years. *Annu. Rev. Mar. Sci.* **13**, 201–226.

MULLER, M., ARBIC, B.K., RICHMAN, J.G., SHRIVER, J.F., KUNZE, E.L., SCOTT, R.B., WALLCRAFT, A.J. & ZAMUDIO, L. 2015 Toward an internal gravity wave spectrum in global ocean models. *Geophys. Res. Lett.* **42**, 3474–3481.

MURRAY, B. & BUSTAMANTE, M.D. 2018 Energy flux enhancement, intermittency and turbulence via fourier triad phase dynamics in the 1-D Burgers equation. *J. Fluid Mech.* **850**, 624–645.

NAZARENKO, S. 2011 *Wave Turbulence*. Springer.

OHKITANI, K. & KIDA, S. 1992 Triad interactions in a forced turbulence. *Phys. Fluids* A **4**, 794–802.

PARESCHI, L. & RUSSO, G. 2005 Implicit-explicit Runge–Kutta schemes and applications to hyperbolic systems with relaxation. *J. Sci. Comput.* **25**, 129–155.

POLLMANN, F. 2020 Global characterization of the ocean's internal wave spectrum. *J. Phys. Oceanogr.* **50**, 1871–1891.

POLVANI, L.M., MCWILLIAMS, J.C., SPALL, M.A. & FORD, R. 1994 The coherent structures of shallow-water turbulence: deformation-radius effects, cyclone/anticyclone asymmetry and gravity-wave generation. *Chaos* **4**, 177–186.

REMMEL, M. & SMITH, L. 2009 New intermediate models for rotating shallow water and an investigation of the preference for anticyclones. *J. Fluid Mech.* **635**, 321–359.

RENAUD, A., VENAILLE, A. & BOUCHET, F. 2016 Equilibrium statistical mechanics and energy partition for the shallow water model. *J. Stat. Phys.* **163**, 784–843.

REZNIK, G.M. 2015 Wave adjustment: general concept and examples. *J. Fluid Mech.* **779**, 514–543.

SALMON, R. 1978 *Lectures on Geophysical Fluid Dynamics*. Oxford University Press.

SHCHERBINA, A.Y. *et al.* 2015 The latmix summer campaign: submesoscale stirring in the upper ocean. *Bull. Am. Meteorol. Soc.* **96**, 1257–1279.

SOH, H.S. & KIM, S.Y. 2018 Diagnostic characteristics of submesoscale coastal surface currents. *J. Geophys. Res.* **123**, 1838–1859.

SUANDA, S.H., FEDDERSEN, F., SPYDELL, M.S. & KUMAR, N. 2018 The effect of barotropic and baroclinic tides on three-dimensional coastal dispersion. *Geophys. Res. Lett.* **45**, 11235–11246.

THOMAS, J. & DANIEL, D. 2020 Turbulent exchanges between near-inertial waves and balanced flows. *J. Fluid Mech.* **902**, A7.

THOMAS, J. & DANIEL, D. 2021 Forward flux and enhanced dissipation of geostrophic balanced energy. *J. Fluid Mech.* **911**, A60.

THOMAS, J. & GUPTA, A. 2022 Wave-enhanced tracer dispersion. *J. Geophys. Res.* **127**, e2020JC017005.

VALLIS, G.K. 2006 *Atmospheric and Oceanic Fluid Dynamics*. Cambridge University Press.

VANNESTE, J. 2013 Balance and spontaneous wave generation in geophysical flows. *Annu. Rev. Fluid Mech.* **45** (1), 147–172.

WALEFFE, F. 1992 The nature of triad interactions in homogeneous turbulence. *Phys. Fluids* A **4**, 350–363.

WARD, M.L. & DEWAR, W.K. 2010 Scattering of gravity waves by potential vorticity in a shallow-water fluid. *J. Fluid Mech.* **663**, 478–506.

WARN, T. 1986 Statistical mechanical equilibria of the shallow water equations. *Tellus* A **38A**, 1–11.

XIA, H., FRANCOIS, N., PUNZMANN, H. & SHATS, M. 2019 Tunable diffusion in wave-driven two-dimensional turbulence. *J. Fluid Mech.* **865**, 811–830.

YEUNG, P.K. & BRASSEUR, J.G. 1991 The response of isotropic turbulence to isotropic and anisotropic forcing at the large scales. *Phys. Fluids* A **3**, 884–897.

YOKOYAMA, N. 2004 Statistics of gravity waves obtained by direct numerical simulation. *J. Fluid Mech.* **501**, 169–178.

YOO, J.G., KIM, S.Y. & KIM, H.S. 2018 Spectral descriptions of submesoscale surface circulation in a coastal region. *J. Geophys. Res.* **123**, 4224–4249.

YUAN, L. & HAMILTON, K. 1994 Equilibrium dynamics in a forced-dissipative f-plane shallow-water system. *J. Fluid Mech.* **280**, 369–394.

ZAKHAROV, V., DIAS, F. & PUSHKAREV, A. 2004 One-dimensional wave turbulence. *Phys. Rep.* **398**, 1.

ZAKHAROV, V.E., L'VOV, V.S. & FALKOVICH, G. 1992 *Kolmogorov Spectra of Turbulence I*. Springer.

ZEITLIN, V. 2018 *Geophysical Fluid Dynamics: Understanding (Almost) Everything with Rotating Shallow Water Models*. Oxford University Press.

ZEITLIN, V., MEDVEDEV, S.B. & POLOUGONVEN, R. 2003 Frontal geostrophic adjustment, slow manifold and nonlinear wave phenomena in one-dimensional rotating shallow water. Part 1. Theory. *J. Fluid Mech.* **481**, 269–290.

ZHOU, Y. 1993 Degrees of locality of energy transfer in the inertial range. *Phys. Fluids* A **5**, 1092–1094.